
AFRL-RX-WP-TR-2011-4213

# TECHNICAL OPERATIONS SUPPORT III (TOPS III)

## Delivery Order 0081: Novel Pitch Materials for High Thermal Conductivity Carbon Fibers, Foams and Composites - Phase III

**Dr. Amod A. Ogale**

**Clemson University**

**JUNE 2011**
**Final Report**



**AIR FORCE RESEARCH LABORATORY**
**MATERIALS AND MANUFACTURING DIRECTORATE**
**WRIGHT-PATTERSON AIR FORCE BASE, OH 45433-7750**
**AIR FORCE MATERIEL COMMAND**
**UNITED STATES AIR FORCE**

# NOTICE AND SIGNATURE PAGE

Using Government drawings, specifications, or other data included in this document for any purpose other than Government procurement does not in any way obligate the U.S. Government. The fact that the Government formulated or supplied the drawings, specifications, or other data does not license the holder or any other person or corporation; or convey any rights or permission to manufacture, use, or sell any patented invention that may relate to them.

This report was cleared for public release by the Wright-Patterson Public Affairs Office and is available to the general public, including foreign nationals. Copies may be obtained from the Defense Technical Information Center (DTIC) (http://www.dtic.mil).

AFRL-RX-WP-TR-2011-4213 HAS BEEN REVIEWED AND IS APPROVED FOR PUBLICATION IN ACCORDANCE WITH ASSIGNED DISTRIBUTION STATEMENT.

*//signature//

KARLA STRONG, Program Manager
Thermal Sciences and Materials Branch
Nonmetallic Materials Division

*//signature//

NADER HENDIZADEH, Chief
Thermal Sciences and Materials Branch
Nonmetallic Materials Division

*//signature//

SHASHI K. SHARMA, Deputy Chief
Nonmetallic Materials Division
Materials & Manufacturing Directorate

This report is published in the interest of scientific and technical information exchange, and its publication does not constitute the Government's approval or disapproval of its ideas or findings.

*Disseminated copies will show "//signature//" stamped or typed above the signature blocks.

# REPORT DOCUMENTATION PAGE

*Form Approved*
*OMB No. 0704-0188*



| 1. REPORT DATE *(DD-MM-YY)* | 2. REPORT TYPE | 3. DATES COVERED *(From - To)* |
|---|---|---|
| June 2011 | Final | 11 August 2009 – 30 March 2011 |

**4. TITLE AND SUBTITLE**
TECHNICAL OPERATIONS SUPPORT III (TOPS III)
Delivery Order 0081: Novel Pitch Materials for High Thermal Conductivity Carbon Fibers, Foams and Composites - Phase III

**5a. CONTRACT NUMBER**
FA8650-05-D-5807-0081

**5b. GRANT NUMBER**

**5c. PROGRAM ELEMENT NUMBER**
62102F

**6. AUTHOR(S)**
Dr. Amod A. Ogale

**5d. PROJECT NUMBER**
4347

**5e. TASK NUMBER**
30

**5f. WORK UNIT NUMBER**
BC104100-C

**7. PERFORMING ORGANIZATION NAME(S) AND ADDRESS(ES)**

Clemson University
203 Earle Hall
Clemson, SC 29634

**8. PERFORMING ORGANIZATION REPORT NUMBER**

**9. SPONSORING/MONITORING AGENCY NAME(S) AND ADDRESS(ES)**

Air Force Research Laboratory
Materials and Manufacturing Directorate
Wright-Patterson Air Force Base, OH 45433-7750
Air Force Materiel Command
United States Air Force

**10. SPONSORING/MONITORING AGENCY ACRONYM(S)**
AFRL/RXBT

**11. SPONSORING/MONITORING AGENCY REPORT NUMBER(S)**
AFRL-RX-WP-TR-2011-4213

**12. DISTRIBUTION/AVAILABILITY STATEMENT**
Approved for public release; distribution unlimited.

**13. SUPPLEMENTARY NOTES**
PAO case number 88ABW-2011-3689, cleared 27 June 2011. Report contains color.

**14. ABSTRACT**

The overall goal of this project was to control nanotexture of pitch precursors by the introduction nanomodifiers of different aspect ratios, thereby modifying the structure of the resulting fibers. The specific objectives were to: (i) Characterize the dispersion of nanoparticles and the microstructure of the fibers; (ii) Quantify the effect of nanomodification on fiber mechanical properties; and (iii) Develop an experimental protocol to measure and model the high thermal conductivity of such carbon fibers based on their composites. The use of melt mixing was confirmed to be an acceptable method for dispersing carbon nanomodifiers such as SAR MWCNT and carbon black into a mesophase pitch matrix. A method for capturing high-speed images of a carbon fiber during the single-filament tensile recoil test was established. Finite element analysis was used to simulate laser flash analysis on unidirectional carbon fiber-epoxy composites.

**15. SUBJECT TERMS**
carbon fibers, pitch precursors, nanomodifiers, thermal conductivity

| 16. SECURITY CLASSIFICATION OF: | | | 17. LIMITATION OF ABSTRACT: | 18. NUMBER OF PAGES | 19a. NAME OF RESPONSIBLE PERSON (Monitor) |
|---|---|---|---|---|---|
| a. REPORT | b. ABSTRACT | c. THIS PAGE | | | Karla Strong |
| Unclassified | Unclassified | Unclassified | SAR | 34 | 19b. TELEPHONE NUMBER *(Include Area Code)* N/A |

**Standard Form 298 (Rev. 8-98)**
Prescribed by ANSI Std. Z39-18

# TABLE OF CONTENTS

**Section** **Page**

# LIST OF FIGURES

**Figure** **Page**

# LIST OF TABLES

**Table** **Page**



# ACKNOWLEDGEMENTS

The authors gratefully acknowledge Dr. Karla Strong (AFRL project monitor), Dr. Tia Benson-Tolle, and Dr. David P. Anderson for their help on various aspects of this project. This work made use of ERC Shared Facilities supported by the National Science Foundation under Award Number EEC-9731680.

## 1.0 INTRODUCTION

High thermal conductivity carbon materials have attracted attention in aerospace applications that are performance driven (e.g., satellites, space shuttle leading edges). The next challenge with such advanced carbon materials lies in making them **multi-functional** such that high thermal conductivity is also accompanied by sufficient strength. Further, for structural purposes, there also needs to be a balance between tensile and compressive properties. An efficient nanostructural control of the fibers and microstructural control of the final carbon product is necessary to provide these multi-functional properties.

Carbon fibers produced from discotic nematic pitch, often called "mesophase pitch", display a thermal conductivity that is about three times that of copper [1-3]. The liquid crystalline precursor consists of polynuclear aromatic hydrocarbons that lead to highly graphitic carbon fibers. The planar, disk-like molecular architecture facilitates three-dimensional graphitic crystal formation, which leads to the ultrahigh thermal conductivity of over 1100 W/m.K. However, this highly crystalline structure is extremely flaw-sensitive and leads to a very brittle fiber that displays a very low strain-to-failure and a poor compressive strength of 0.5 to 0.7 GPa due to microbuckling of super-aligned graphene layers. Such carbon fibers suffer from poor handleability and cannot be used directly in woven or braided forms. Also, such high-performance pitch-based carbon fibers are expensive, some grades available at over $ 1,000 per pound (viz. K1100). This high cost and an imbalance of properties is preventing the wide-spread use of pitch-based carbon fibers in thermal management applications.

A careful control of fiber properties has not been possible because the mesophase pitch (MP) precursor composition and architecture has not been adequately tailored. In prior studies, we have proposed the addition of multi-wall carbon nanotubes to mesophase pitch in an attempt to modify the properties of the resulting carbon fibers [4,5]. The study primarily used long aspect ratio nanotubes and led to an improvement of the ratio of the compressive to tensile strength [6]. However, the thermal and mechanical properties of such fibers have not been systematically investigated as a function of different aspect ratios of the nanomodifiers.

## 2.0 PROJECT GOAL & OBJECTIVE

The overall goal of this project was to control nanotexture of pitch precursors by the introduction nanomodifiers of different aspect ratios, thereby modifying the structure of the resulting fibers. The specific objectives were to:

i. Characterize the dispersion of nanoparticles and the microstructure of the fibers;

ii. Quantify the effect of nanomodification on fiber mechanical properties;

iii. Develop an experimental protocol to measure and model the high thermal conductivity of such carbon fibers based on their composites.

## 3.0 EXPERIMENTAL

### 3.1 Materials

All fibers were produced using ARHP grade mesophase pitch from Mitsubishi Gas Chemical with a measured softening point of 286°C. Nanoparticles used for this study include: short aspect ratio multiwalled carbon nanotubes (SAR MWCNT) and carbon black. Specifications for each of these materials are provided in Table 1, and representative SEM micrographs of these particles are shown in Figure 1.

**Table 1. Nanoparticle Specifications: Size, Purity, and Source**

| Nanoparticle Type | Size | Purity | Source |
|---|---|---|---|
| Short Aspect Ratio MWCNT | d≈10-30 nm, L≈1 μm* | >95%* | SES Research |
| Carbon Black | Agglomerated particles of various sizes | NA | Ketjen Black |

*As specified by supplier

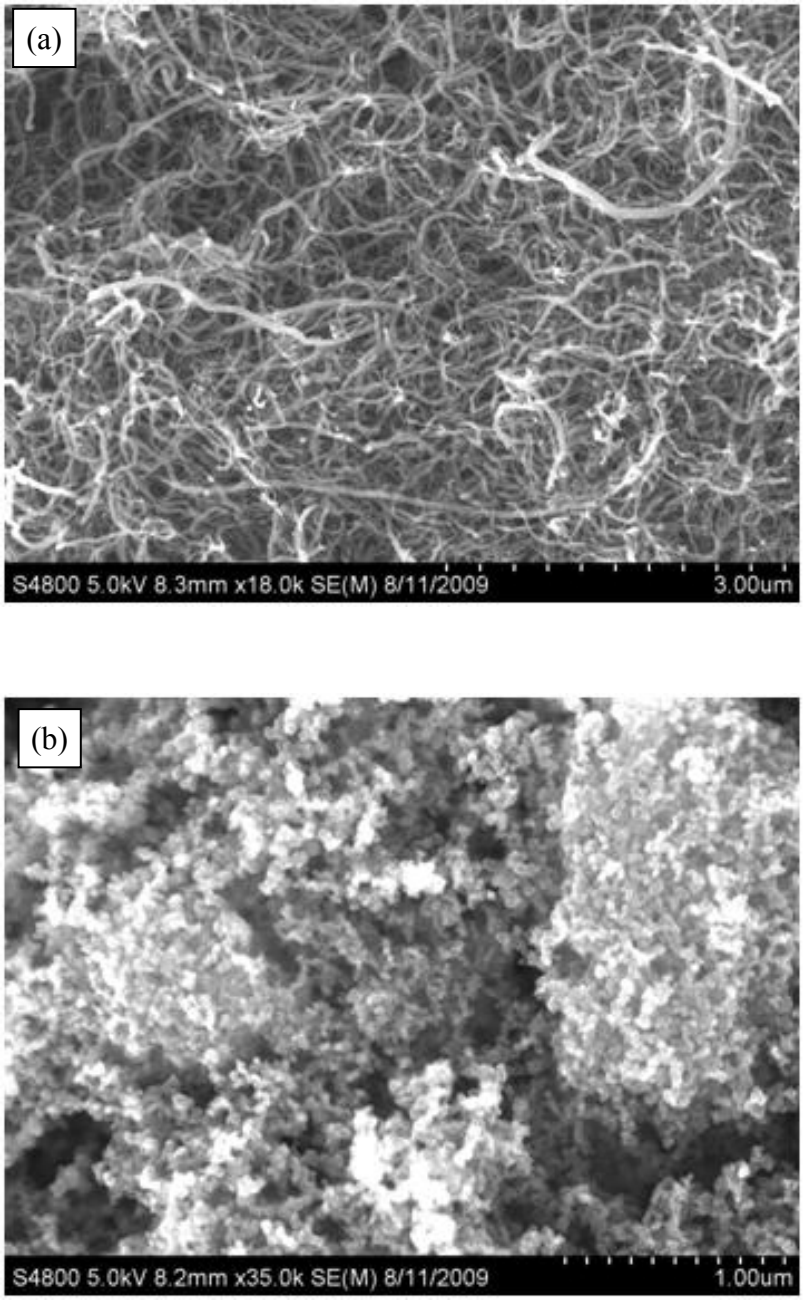


**Figure 1. SEM Images of (a) Short Aspect Ratio (SAR) of Multi-Wall Carbon Nanotubes (MWCNTs) and (b) Carbon Black (CB)**

## 3.2 Processing

### *Dispersion*

Dispersion of nanoparticles was performed using a twin-screw extruder (Model #MP2015, APV Chemical Machinery). The 10 mm diameter co-rotating screws were operated at 30 RPM in conjunction with a 1 mm diameter die with a L/D of 20. All dispersion studies were done in a nitrogen atmosphere to limit oxidative crosslinking and degradation of the mesophase pitch. Temperature control of the extruder was achieved through the use of four heating zones with independently controlled heater bars and thermocouples. From the feed zone to the die, the temperature profile was specified to be: 275, 300, 300, and 305$^{o}$C (±1$^{o}$C). Pressure drop across the die was measured by a pressure transducer located in the last zone. To obtain 0.3 wt% nanomodifier content, the solids were fed in the ratio of 10 grams of pitch for 30 mg of nanoparticles. To enhance dispersion, the material was processed through the extruder three times.

### *Fiber Spinning*

The compounded mixtures were melt-spun into fibers using a constant volumetric flow rate, plunger-and-barrel batch unit (Alex James and Associates, Greenville, SC). All spinning was performed under a nitrogen atmosphere to minimize pitch oxidation. A 12-hole spinneret with 150 μm diameter holes was used throughout. The spinning temperature was between 305 to 310$^{o}$C, and the take-up roller speed was controlled between about 400 and 800 m/min; thinner fibers are produced using the higher take-up speed.

### *Thermal Treatment*

As-spun fibers were thermo-oxidatively stabilized for 48 hours by spreading them on a screen rack in an air convection oven, preheated to 205$^{o}$C. Each sample was carefully weighed before and after oxidation to ensure oxygen uptake of 8 to 10% (mass gain). Then, fibers were graphitized in an Astro 1100 furnace under a helium atmosphere at a maximum temperature of 2600$^{o}$C for 1 hour holding time.

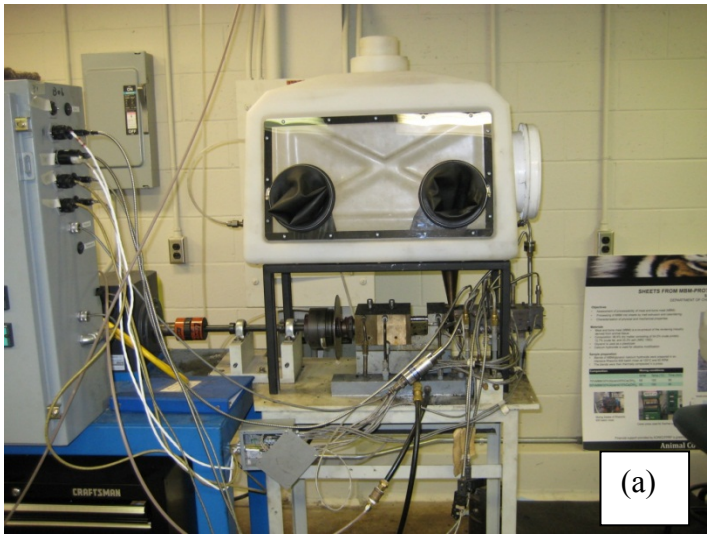


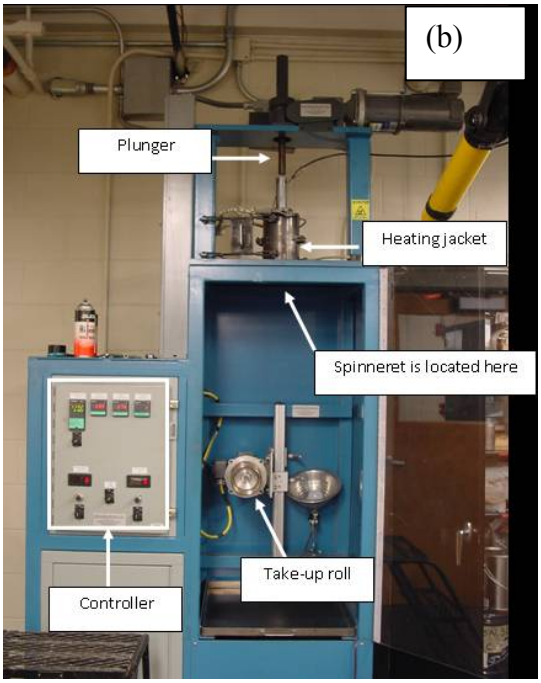


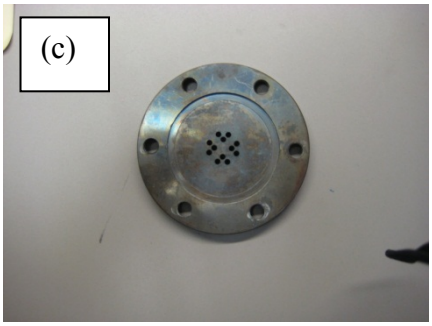


**Figure 2. Melt-Dispersion and Fiber Spinning Equipment: (a) Twin-Screw Extruder used for Melt-Dispersion of Nanomodifiers in Mesophase Pitch; (b) Melt-Spinning unit Consisting of a 37-mm Diameter Barrel and (c) a 12-Hole Spinneret with 150 Micrometer Diameter Holes**

### 3.3 Characterization of Fiber Texture and Microstructure

A field-emission scanning electron microscope (Hitachi S-4800) was used to examine the dispersion of nanoparticles in oxidized pitch fibers and the graphene layer orientation distribution in carbonized fibers. Samples were broken under liquid nitrogen to achieve as a clean a surface as possible, and mounted vertically on stainless steel stubs. Oxidized pitch fibers were sputter coated with gold for 2 minutes to prevent charging in the SEM. Carbonized fibers have sufficiently conductivity that they do not require any coating.

The microstructure of both oxidized and graphitized fibers was also observed using an Olympus BX60 optical microscope with cross-polarizers and a full wave-plate retarder. Fiber samples were adhered vertically to a piece of pre-hardened casting resin, placed in a sample mounting cup, which was then carefully filled with fresh casting resin. The resin was allowed to cure for 1 hour at room temperature and then 24 hours at 70$^{o}$C. Next, samples were polished using progressively finer grit paper on an Ecomet Grinder/Polisher. The average diameter and percentage of carbon fibers which exhibit "pac-man" types splitting was determined from these optical micrographs of fiber cross sections. No fewer than 100 fibers were counted to obtain adequate statistical significance.

Wide angle x-ray diffraction was used to quantify changes in fiber crystallography and orientation due to nanomodification. Milled carbon fibers, mixed with approximately 5 to 10 wt% NIST-certified silicon standard, were analyzed using a Rigaku Ultima IV to obtain estimates of inter-planar spacing ($d_{002}$), crystallite thickness corresponding to stacking height of layer planes ($L_c$), and crystallite length ($L_a$). The silicon standard provided a reference for two-theta positions, as well as a measure of instrument broadening. Fiber tows, hardened by a slurry of Super Glue and NIST silicon standard, were analyzed using Rigaku-MSC to obtain the full-width at half-maximum (FWHM) of the $d_{002}$ azimuthal peak to quantify graphene layer orientation in the fibers.

### 3.4 Mechanical Property Measurement

The tensile and compressive properties of the carbon fibers were quantified using a Phoenix universal testing machine from Measurement Technology, Inc (MIT) with a 500 g load cell at a cross head speed of 0.5 mm/min. Single filaments were mounted on 25 mm gauge length paper tabs with 2 Ton Clear Weld Epoxy, and allowed to dry about 12 hours. Initial fiber diameter measurements for mechanical test were performed using laser diffraction. Later, electron microscopy was used to check for splitting and non-circular fibers, and to determine the cross sectional area of the fiber which is used to calculate fiber tensile strength.

The MTI tensile tester was also used to perform compression tests using the tensile-recoil compressive method [6]. An important addition to the technique is that during compression failure, high-speed video was captured using a Phantom V7.0 camera, the Sigma 50 mm DG Macro lens, and a mobile light source [7]. The video controls of the camera control software enable a careful review of the test footage. From this footage, several frames were selected that highlight the different phases of the test: first contact with the electrical arc, fiber severance, first sign of compressive failure, and the residual fiber after the test. A total of 67 fibers were recorded [7]. The use of the high speed camera drastically enhances the ability to scrutinize the single-filament tensile recoil test. The test assumes that the fiber recoils along its axis when severed, much like a stretched elastic band. This phenomenon is extremely hard to visualize by

the naked eye because of the short duration of the recoil event, less than 60 μs. However, the high speed cinematography has facilitated the capturing of the event [7].

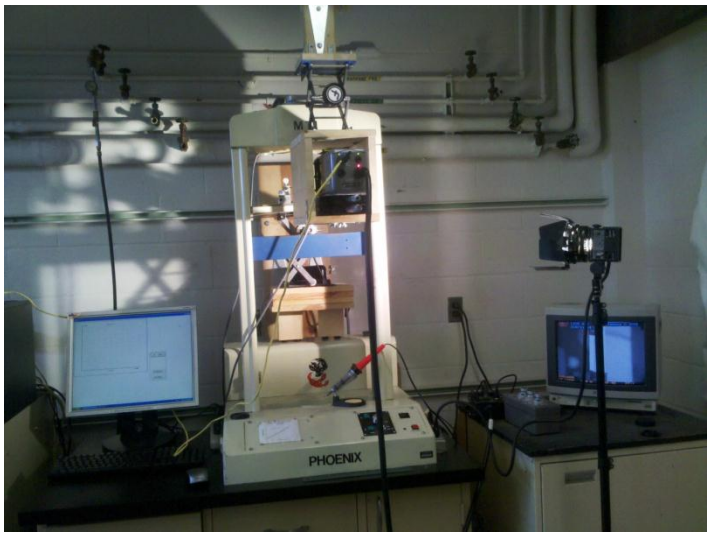


**Figure 3. A Schematic of a Mounted Specimen for Compressive Testing Using a High-Speed Camera for Capturing Tension-Recoil Compressive**

### 3.5 Thermal Conductivity Characterization

The thermal conductivity of carbon fibers was tested using laser flash analysis (LFA) [8]. Samples were made by first embedding in epoxy resin to form unidirectional composites block and then sectioned into 10 mm x 10 mm square disks of approximately 1 or 2 mm thickness. These disks were then vapor coated on both sides with a thin layer of silver to prevent flash through and further sprayed with graphite powder for even lateral heat distribution. Four samples of each fiber type were then analyzed at room temperature using a Netzsch LFA 447 located at Clemson University, which provides a diffusivity ($\alpha_c$) value for the entire composite specimen [9]. Samples were also tested on a Netzsch LFA 457 located at the Air Force Research Labs.

Fiber thermal conductivity ($k_c$) was calculated using equations 1-3. Composite heat capacity ($C_c$) was measured using a Perkin Elmer Pyris 1 DSC, and density ($\rho_c$) was calculated using a balance and volume displacement. Fiber and matrix volume fractions ($v_f$ and $v_m$) were determined using optical microscopy. The fiber thermal conductivity ($k_f$, W/m*K) was also estimated from the electrical resistivity values (p, μΩ*cm) using the empirical Lavin-Izzi correlation listed below [10].

$$k_f = [440,000/(p + 258)] - 295$$

## 4.0 RESULTS AND DISCUSSION

### 4.1 Texture and Microstructure

***Oxidized Pitch Fibers***

Figures 4 through 6 show images of an unmodified pitch fiber (0 wt%), a pitch fiber containing 0.3 wt% SAR MWCNT, and pitch fiber containing 0.3 wt% carbon black, respectively. The SAR MWCNTs show up as bright dots on the fractured surface, the majority being less than 100 nm in diameter. This suggests that the SAR MWCNTs are well dispersed within the pitch matrix. Additionally, the nominal circular shape of the bright dots is evidence that the nanotubes align along the axis of the fiber during spinning. In less than two percent of fibers, micrometer size bundles of SARMWCNT were discovered.

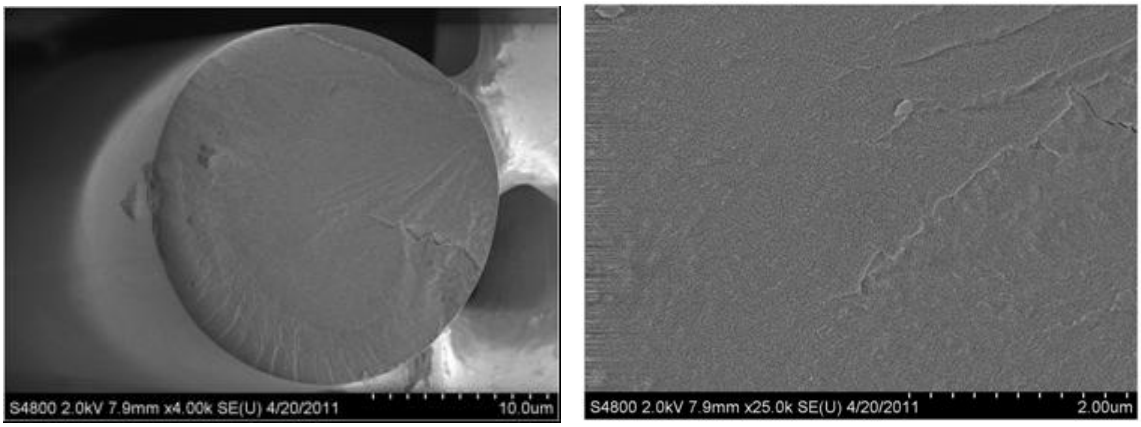


**Figure 4. SEM Images of Oxidized 0 wt% ARHP Mesophase Pitch Fibers; Left-Side Image at Lower Magnification and Right-Side at Higher Magnification**

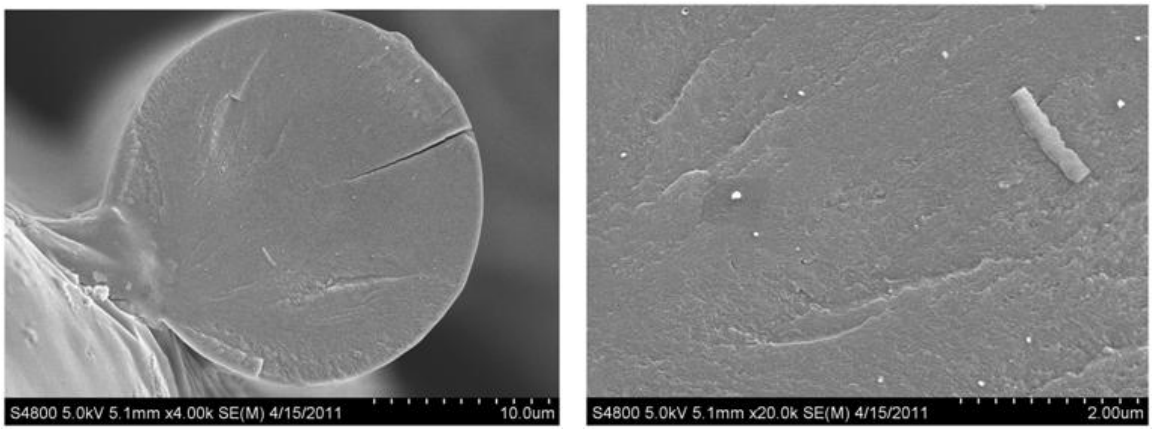


**Figure 5. SEM Images of Oxidized ARHP Mesophase Pitch Fiber Containing 0.3 wt% SAR MWCNT**

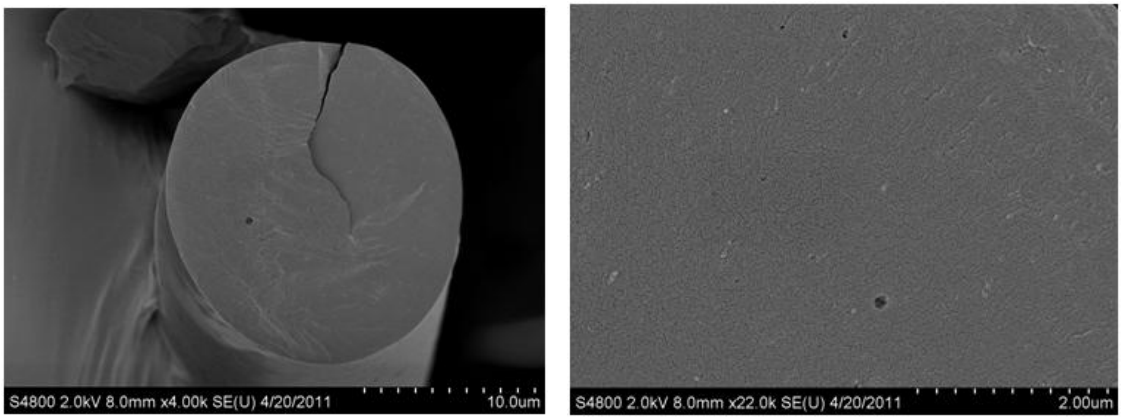


**Figure 6. SEM Images of Oxidized ARHP Mesophase Pitch Fiber Containing 0.3 wt% Carbon Black**

The carbon black modifiers were more difficult to spot because they provide little contrast from the mesophase pitch matrix. Only under high magificantion do the particle agglomerations appear as light grey spots against the darker grey mesophase pitch matrix, the majority of having diameters of between 50 to 100 nm. A few particle agglomerations on the order of 100 to 500 nm were observed.

Changes in the cross sectional orientation of the mesophase pitch matrix due to the nano-inclusions are apparent from images taken using cross polarize light microscopy. The 0 wt% fibers show a radial orientation of the mesophase (Figure 7(a)). However for the nanomodified fibers, this structure appears disrupted, and the mesophase domains are marble across the fiber cross section. No spitting is observed in any fibers prior to oxidation.

Wide-angle x-ray diffraction results indicate that the FWHM for the 0 wt%0 wt%, 0.3 wt% SAR MWCNT and 0.3wt% carbon black are 28.9°±0.6°, 30.2°±0.7° and 29.4°±0.5°, respectively. These azimuthal data from as-spun pitch fibers shows no signification change in axial orientation due to the addition of SAR MWCNT or carbon black.

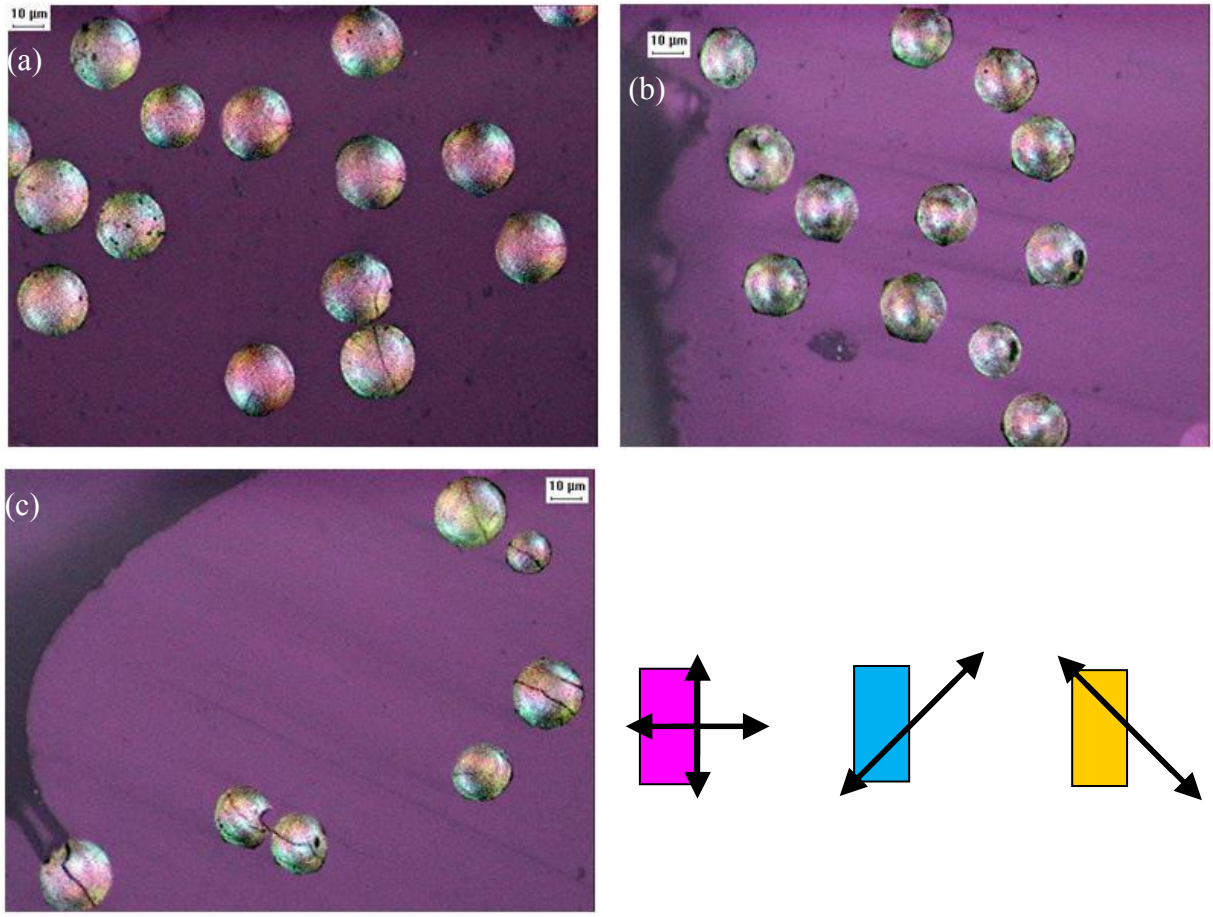


**Figure 7. Optical Images of Oxidized Mesophase Pitch Fibers Contain (a) 0 wt%, (b) 0.3 wt% SAR MWCNT and (c) 0.3wt% Carbon Black Taken Using a Light Microscope with Cross Polarizing Filter and a Full Wave-Plate Retarder**

### *Carbon Fibers*

SEM micrograph of experimental carbon fibers, presented in Figure 8(a), provides a detailed view of the radial orientation of graphite planes around the fiber axis for a split 0 wt% carbon fiber. In contrast, carbon fibers containing 0.3 wt% SAR MWCNTs [Figure 8(b)] and 0.3 wt% carbon black [Figure 8(c)] exhibit a modified Pan Am structure. In many of the fibers containing carbon black, the distortion of the structure causes the fiber to adopt a egg shaped cross section.

Optical micrographs of typical 0 wt%, 0.3 wt% SAR MWCNT and 0.3 wt% carbon black carbon fibers are presented in Figure 9. The 0 wt% fibers have an average diameter (±95% CI) of 17.3±0.3 µm and 85% show splitting. Those carbon fibers modified with 0.3 wt% SAR MWNCT have an average diameter (±95% CI) of 17.2±0.5 µm and 5% show splitting. Those carbon fibers modified with 0.3 wt% carbon have an average diameter (±95% CI) of 16.7±0.5 µm and 55% show splitting. By comparing cross polarized micrographs, it can be observed that the addition of SAR MWCNTs or carbon black also corresponds with a blurring of the radial microstructure present in the 0 wt% carbon fibers.

In contrast to as-spun pitch fibers, the azimuthal data from the carbonize fibers shows that the presence of nanoparticles slightly decreases axial orientation. The FWHM for the 0 wt%0 wt%, 0.3 wt% SAR MWCNT and 0.3 wt% carbon black are 2.8°±0.1°, 4.2°±0.1° and 4.5°±0.1°.

Furthermore, the presence of SAR MWCNT slightly increases the d-spacing slightly to 3.383±0.001 Å from 3.378±0.001 Å for the 0 wt%. However, the difference between the d-spacing of the 0 wt% carbon fibers and those containing 0.3 wt% carbon black (3.379±0.001 μm) was not significant statistically.

Additionally, through-plane crystallite size of fibers containing 0.3 wt% SAR MWCNT was slightly smaller (25.7±0.1 nm) than that of the 0 wt% fiber (29.2±0.2 nm). However, there was no statistically significant difference between the through plane crystallite size of the 0 wt% carbon fibers and those containing 0.3 wt% carbon black (30.0±0.8 nm). Furthermore, no change in the in-plane crystallite size was observed from the addition of SAR MWCNT and carbon black resulted due to the large uncertainty in these measurements.

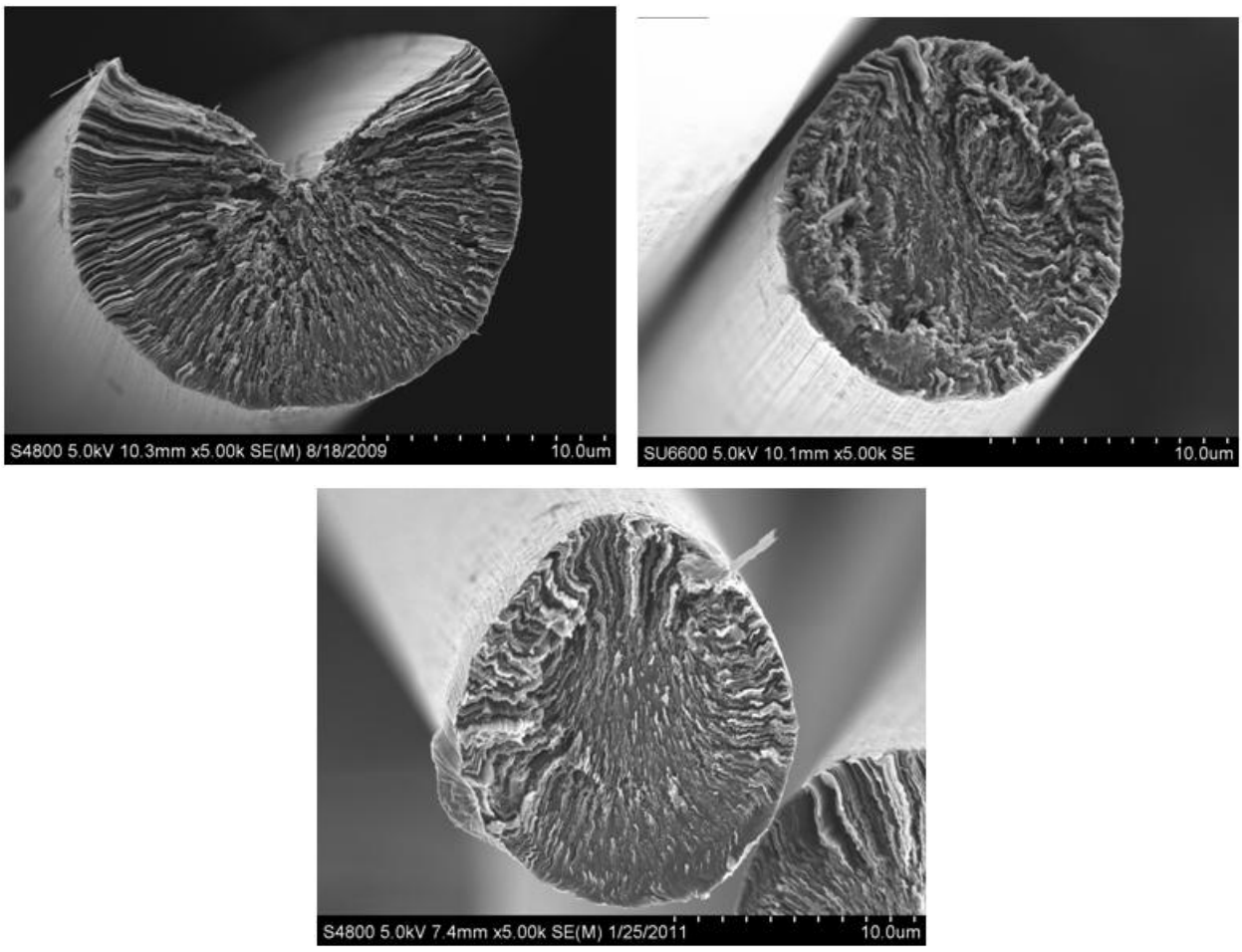


**Figure 8. SEM Micrographs of Carbon Fibers Containing (a) 0 wt%, (b) 0.3 wt% SAR MWCNT and (c) 0.3wt% Carbon Black**

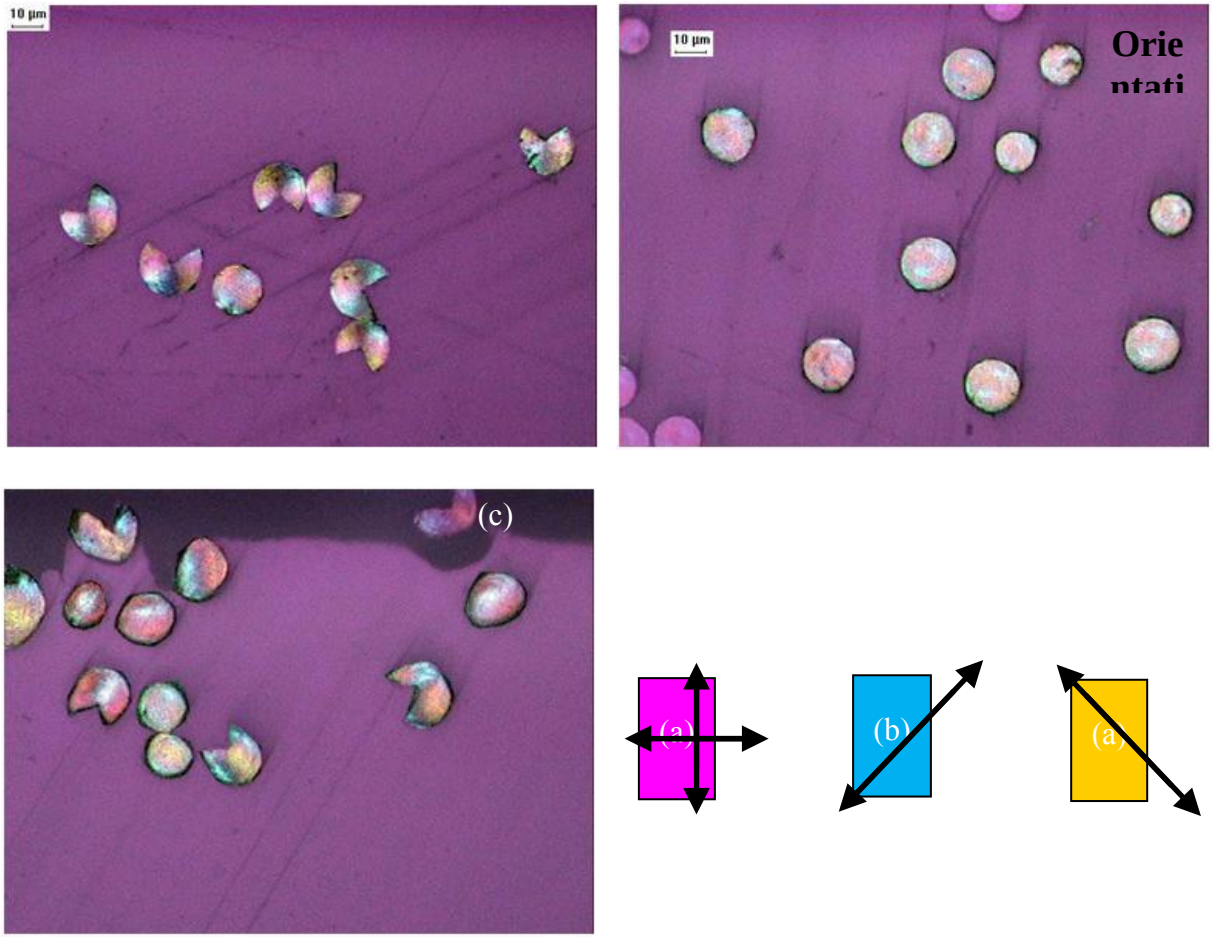


**Figure 9. Optical Microscopy Images (with Cross Polarizing Filter and a Full Wave-Plate Retarder) of Carbon Fibers Containing (a) 0 wt%, (b) 0.3 wt% SAR MWCNT and (c) 0.3wt% Carbon Black**

### 4.2 Mechanical Properties

The tensile properties of pitch-based carbon fibers are difficult to quantify due to their brittle nature. Of the unmodified or "control" (0 wt%) carbon fibers mounted, only about one-third could be tested. The average diameter, tensile strength, strain-to-failure and tensile modulus were 16.7±0.6 µm, 1590±220 MPa, 0.28±0.05%, 580±60 GPa. Of the fibers that could not be tested, about 40% broke prior to testing, 35% broke prematurely while slack was being removed from the fiber during testing (six with radial splitting) and 25% showed signs that they slipped out of position in the epoxy. The compressive strength of 0 wt% fibers was measured to be approximately 790 MPa.

Of the carbon fibers containing 0.3 wt% SAR MWCNTs mounted, 55% (none split) could be successfully tested. The average diameter of these fibers (16.0±0.6 µm) is not statistically significant from the 0 wt% fibers, and therefore tensile properties can be compared without concern for size effects. The tensile strength (1220±140 MPa) and strain- to-failure (0.25±0.04 %) of the 0.3 wt% SAR MWCNTs are slightly less than the 0 wt% fiber. However, the lower tensile modulus (490±40 GPa), in combination with the higher compressive strength (> 825

MPa), explain the better handleability of the fibers containing the SAR MWCNTs. Only one fiber broke prior to testing, none broke prematurely and seven showed signs that they slipped out of position in the epoxy.

Of the carbon fibers containing 0.3 wt% carbon black, 60% could be successfully tested. Fiber diameter and cross sectional area data have not been corrected for fiber splitting. The average diameter (18.6±2.1 μm) measured using optical microscope over-predicts the true corrected diameter. Both the tensile strength (930±250 MPa) and modulus (370±40 GPa) are most likely under-predicted due to this same error, as both require fiber diameter in their calculations. Compressive strength of carbon fibers containing 0.3 wt% carbon black could not be completed; these will be tested in a future study.

### 4.3 Thermal Conductivity

#### *Thermal Flash and ER Measurements*

As reported earlier, thermal conductivity values of the unmixed, 0 wt% , and 0.3 wt% MWCNT-modified carbon fibers measured using both the thermal-flash and single filament (electrical resistivity correlation) methods are presented in Figure 10 [9]. The "unmixed" material, which has undergone no melt mixing and has no nanoparticle inclusions, displayed a thermal conductivity of 350 ±130 W/m*K as calculated from the thermal flash technique and 520 ±70 W/m*K as calculated from the electrical resistivity correlation method. For all three fiber types, the electrical resistivity method predicts a thermal conductivity that is approximately 200 W/m*K higher than that measured from the LFA method. These results may be explained as the difference between the measurement taken on a nearly perfect single filament versus that taken on a bulk sample of fibers were some fiber can be damaged or disoriented thus lowering the average conductivity.

A comparison of the thermal conductivity of different fibers, calculated using the electrical resistivity correlation, for the unmixed (520±70 W/m*K) and 0 wt% (570±40 W/m*K) showed no statistical difference from each other or from the 0.3 wt% MWCNT sample (550±30 W/m*K). This is consistent with data from those obtained from the LFA technique, which also showed that the conductivity of 0.3 wt% MWCNT (330±120 W/m*K) fibers had not reduced significantly from that of the 0 wt% fibers (350±130 W/m*K).

To investigate the difference between conductivity values calculated from unidirectional heat transport assumption inherent to the composite method and those obtained from electrical resistivity data, a finite element modeling (FEM) study was conducted. For nonhomogeneous materials, such as carbon foams, prior FEM studies have proven that thermal transport can occur preferentially conduct through the highly conductive carbon struts [11].

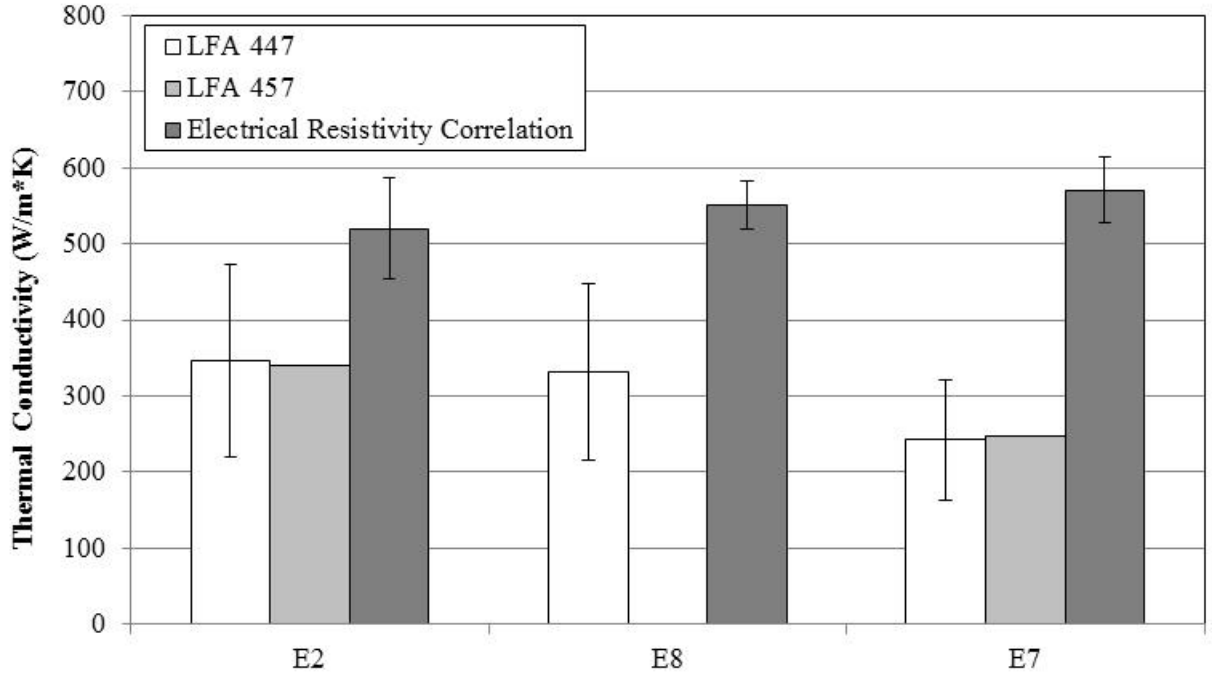


**Figure 10. Thermal Conductivity of Unmixed (E2), 0 wt% (E8), and 0.3 wt% MWCNT Modified (E7) Carbon Fibers Measured Using Laser Flash Analysis (LFA 447 & LFA 457) and Predicted from Electrical Resistivity Measurements Using an Empirical Correlation**

### 4.4 Modeling

PDEFlex software (www.pdesolutions.com) was used to develop an FEM of the unsteady-state heat flow through a unidirectional carbon fiber-epoxy composite. To simplify computations, a single fiber surrounded by a polymer matrix was chosen as the representative volume element (RVE). The actual test specimen is made up of thousands (to millions) of such RVEs along the lateral directions (Fig. 11), but calculations are required for only one such element if the composite geometry is simplified as an array of fibers evenly packed within the matrix. This effectively creates a condition of symmetry in temperature profile at the boundary of each element and along the axis of each fiber. Therefore, a 2-D axisymmetric model of a single fiber surrounded by a polymer matrix was used for this work, with adiabatic boundary conditions of the vertical surfaces (R = 0 and 5 + $L_m$ μm). Horizontal boundary conditions (Z = 0 and L + 2*$L_{gs}$) were also specified to be adiabatic, as it was assumed that little heat loss would occur at these surfaces due to short measurement times and low conductivity of air surrounding the sample.

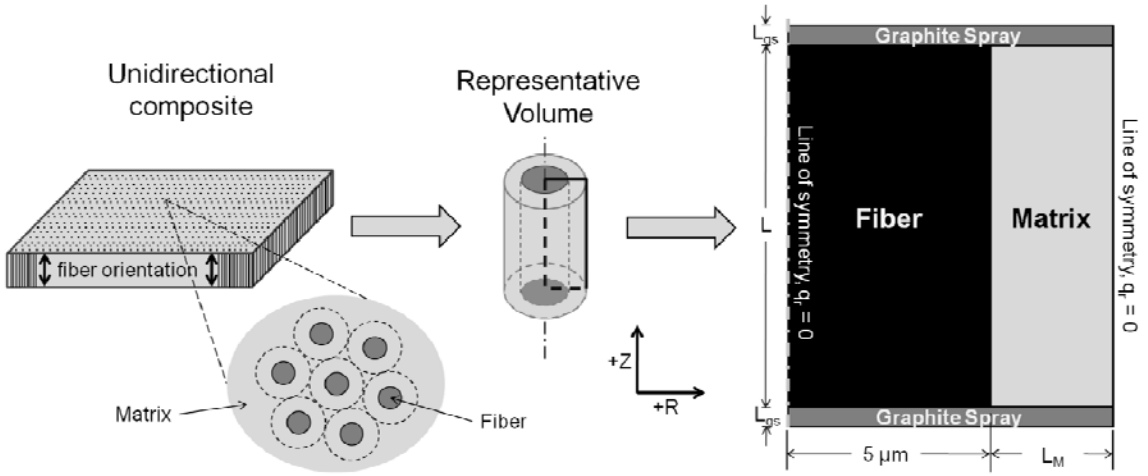


**Figure 11. Multi-Scale Representation of a Larger Uniaxial Composite Showing a Single Fiber and Matrix as the Representative Volume Element (RVE); Symmetry Conditions Reduce the RVE to a 2-D Geometry Shown on the Right**

Typical of pitch-based carbon fibers, a fiber radius of 5 µm, was used throughout this analysis. Fiber content was varied by changing the thickness of the matrix layer ($L_M$) in the radial direction. For each fiber type, five different values of fiber content (0, 10, 20, 60 and 100 % volume) were modeled. Samples of 0 and 100% fiber content corresponded to homogenous materials having properties equivalent to that of pure polymer and carbon fiber, respectively.

The two-dimensional, unsteady-state heat transfer equation (Eq. 1), was the basis for the FE analysis. The density (ρ), heat capacity (C), radial ($k_R$) and axial ($k_Z$) thermal conductivity values were specified as input parameters for the three materials (fiber, matrix, and graphite spray).

$$\rho C \frac{\partial T}{\partial t} + \underline{\nabla} \bullet -\left(\underline{\underline{k}} \bullet \underline{\nabla} T\right) = 0 \qquad (1)$$

The polymer matrix of was assigned a heat capacity ($C_m$) of 2 J/g*K, and a density ($\rho_m$) of 1 g/cm$^3$ and an isotropic thermal conductivity ($k_m = k_{m,R} = k_{m,Z}$) of 0.1 W/m*K throughout, which corresponds to a matrix thermal diffusivity of 0.05 mm$^2$/s. Modeling results were found to be relatively insensitive to small changes in the material properties chosen for the matrix. For the fibers, a heat capacity ($C_f$) of 1 J/g*K and a density ($\rho_f$) of 2 g/cm$^3$ was used. Fibers were assigned different thermal conductivity values: 10, 100 and 1000 W/m*K, which correspond to fiber thermal diffusivity values of 5, 50, and 500 mm$^2$/s. These are comparable to the range of axial conductivity values for pitch-based carbon fibers. However, it is known that carbon fibers can exhibit extremely anisotropic thermal properties ($k_{f,Z} \neq k_{f,R}$). To quantify the effects on LFA measurements due to this anisotropy, a fourth fiber was assigned an axial conductivity of 1000 W/m*K (equivalent axial thermal diffusivity of 500 mm$^2$/s) and a radial conductivity of 10 W/m*K (equivalent radial thermal diffusivity of 5 mm$^2$/s.)

Once FE analysis computations were complete, the data were analyzed to obtain predicted fiber conductivity values. This was achieved by first determining $t_{1/2}$ from simulated LFA curves (a plot of plotting the top surface ($Z = Z_{max}$) temperature, normalized with respect to the equilibrium temperature ($T/T_{EQ}$), versus time after model initialization). Then Eq. (1) was used to determine a predicted composite thermal diffusivity ($\alpha_c = \alpha_s$). The composite conductivity was calculated using Eq. (2), where the density ($\rho_c = \rho_s$) and heat capacity ($C_c = C_s$) are those of the composite. These values were calculated from the model input parameters of pure component density, heat capacity, volume fraction ($v_f$ and $v_m$) and mass fraction values ($m_f$ and $m_m$), using rule-of-mixtures:

$$\rho_c = \rho_f v_f + \rho_m v_m \tag{2}$$

$$C_c = C_f m_f + C_m m_m \tag{3}$$

Finally, the predicted fiber thermal conductivity ($\kappa_f$) was obtained from the predicted composite conductivity, specified matrix conductivity ($k_m$) and specified matrix and fiber volume fraction values, using rule-of-mixtures:

$$\kappa_c = \kappa_f v_f + k_m v_m \Rightarrow \kappa_f = \left(\kappa_c - k_m v_m\right)/v_f \tag{4}$$

Additionally, the agreement of the model results with assumptions of the LFA method (adiabatic boundaries, 1-D heat flow) was verified by normalizing sampling times with their respective half-time values, and then plotting the normalized temperature ($T/T_{EQ}$) versus normalized time ($t/t_{1/2}$). As discussed by Parker et al. [8], LFA curves normalized using this method should all collapse down into a single curve, regardless of the sample conductivity, given that the assumptions of adiabatic boundary conditions and 1-D heat flux are valid. For input fiber thermal conductivities of $k_s$ = 0.1, 10, 100 and 1000 W/m*K, the values predicted from FE analysis were $\kappa_s$ = 0.100, 9.96, 99.0 and 971 W/m*K, for a 1 mm thick sample.

Once verified, the FEM was used to simulate laser flash analysis on composite samples. Fig. 12(a) shows the simulated LFA curves for composites containing the highest conductivity isotropic fiber ($k_f$ = 1000 W/m*K) at 10, 20 and 60% fiber content, as well as the homogenous sample (100%) having material properties equivalent to that of the fiber. One interesting feature of these curves is that the initial top surface temperature rise of the sample containing 10% fiber content is nearly identical to that of the 20% fiber content sample. However, just before 1 ms the top surface temperature rise of the 10% fiber content sample slows dramatically, causing it to diverge from the 20% fiber content sample curve. Furthermore, when the half-time values are used to create curves with a normalized time axis (Fig. 2(b)), their shape is found to be highly dependent on fiber content. The lowest fiber content sample deviates most radically from the homogeneous sample. However, as fiber content increases to 60%, the composite curve almost exactly overlays that for the homogeneous sample. Based on the discussion in the data analysis section, any difference in the shape of the $T/T_{EQ}$ vs. $t/t_{1/2}$ curve generated by a composite material, from that of a homogeneous sample, suggests some deviation from the simple one dimensional heat flow assumed in the development of Eq. (1).

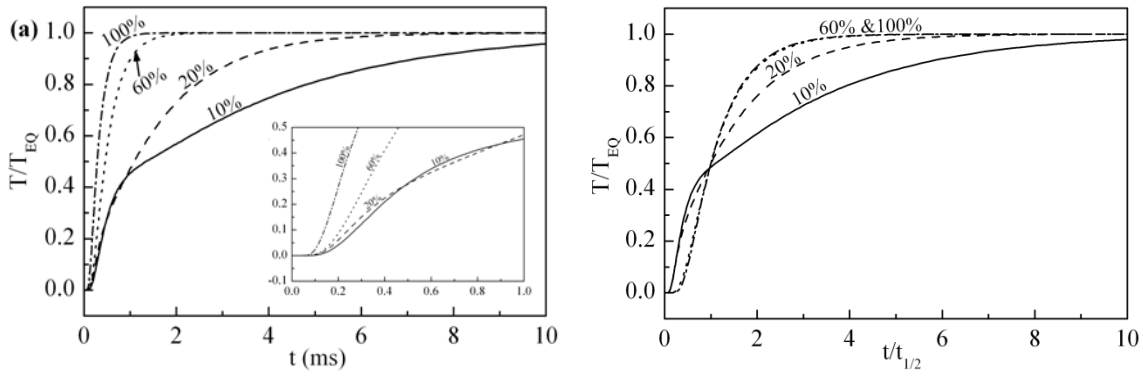


**Figure 12. (a) Simulated LFA Curves for $k_f$ = 1000 W/m*K and L = 1 mm ($v_f$ = 10, 20, 60, 100%) (b)$T/T_{EQ}$ vs. $t/t_{1/2}$ curves for $k_f$ = 1000 W/m*K and L = 1 mm ($v_f$ = 10, 20, 60, 100%)**

For a better understanding of the simulation results the transient temperature profiles were examined. Initially (t = 0), energy was supplied to the lower graphite layer causing a strong z-direction temperature gradient but none in the r-direction. As time progresses, heat began to flow in the positive z-direction, most rapidly through the fiber, but also into the lower regions of the matrix. The difference in conductivity between the fiber and matrix meant that the fiber reached a relatively more uniform temperature through the thickness of the sample far more quickly than the matrix. This caused a relative hotspot in the lower regions of the matrix. Fig. 13(a) shows an example temperature profile at $t/t_{1/2} = 2$ for the 10% fiber content composite.

The sharp radial temperature gradient that developed between the fiber and warmer matrix in the lower part of the sample caused some of the energy to be drawn from the matrix region into the fiber. The heat then flowed through the fiber to the cooler upper part of the composite where it was radially dissipated into the matrix. Additionally, some of the heat flowed in a negative z-direction from the matrix hotspot down into the lower graphite spray layer, radially to the region below the fiber and then up the fiber, as before. For the 10% fiber content sample, this heat flow pattern resulted in the rapid initial temperature rise shown in Fig. 12(a). Meanwhile, the remainder of the heat trapped within the matrix continued to propagate in the positive z-direction, resulting in the slower rise which occurred at later times.

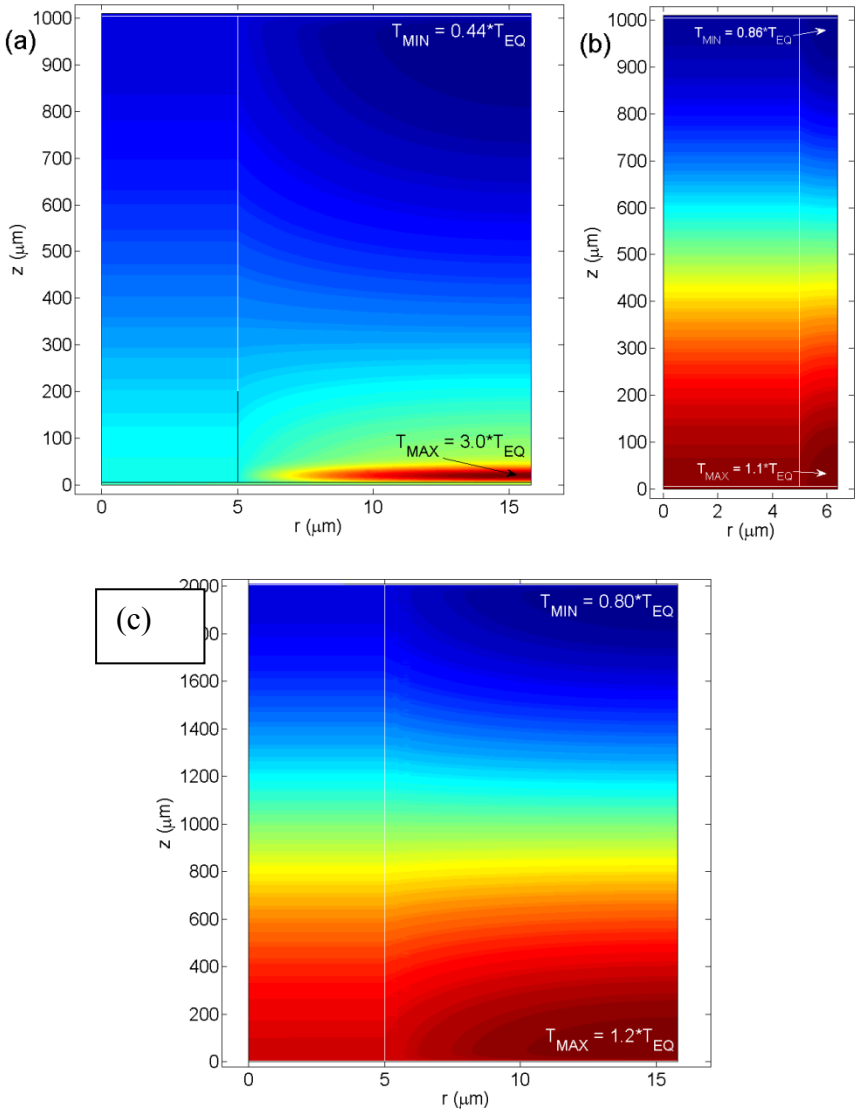


**Figure 13. R vs. Z Temperature Profiles at $t/t_{1/2} = 2$ for a Composite (a) 1 mm Thick, 10% Fiber Content, $k_f$ = 1000 W/m*K, (b) 1 mm Thick, 60% Fiber Content, $k_f$ = 1000 W/m*K, and (c) 2 mm Thick, 10% Fiber Content, $k_f$ = 1000 W/m*K. To Obtain Maximum Color Contrast Each Plot is Scaled to its Maximum and Minimum Temperature, and these Values are Labeled at the Appropriate Locations on the Plot**

As the fiber content increased, the relatively smaller matrix layer around the fiber held less energy in the lower region and required less energy for heating of the upper region. For this reason, the radial gradients between fiber and matrix were far smaller, and the majority of heat flow was in the positive z-direction. Fig. 13(b) shows a typical temperature profile at $t/t_{1/2} = 2$ for the 60% fiber content composite. As a result, the curve in Fig. 12(b) for the 60% fiber content

composite looks very similar to that of the homogeneous sample, which only exhibited z-direction heat flow.

Furthermore, as fiber conductivity decreased, the heat transport through the fiber progressed at a slower speed relative to that for a higher conductivity fiber. This allowed more time for heat to be transferred in the radial direction between the fiber and the resin. Thus, at any given time and z-position, there was a smaller a radial temperature gradient for composites containing the lowest conductivity fiber, compared to those containing higher conductivity. Therefore, the net heat flow for these low conductivity fiber composites more closely resembles that present in homogenous materials. As a result, the simulated LFA data for the 10, 20 and 60% fiber content composites show no overlapping of the data; the $T/T_{EQ}$ vs. $t/t_{0.5}$ curves are indistinguishable from that of the comparative homogenous (100%) material.

Table 2 summarizes the fiber thermal conductivity values predicted from the FE analysis data, using Eq. (1-5). For composites containing fibers of lower conductivity or higher fiber content, the predicted and specified fiber thermal conductivity values are nearly identical However, for composites containing higher conductivity fibers at lower values of fiber content (10 and 20%), the predicted fiber thermal conductivity value is significantly higher than that specified in the model. Again this error resulted from the preferential conduction through the carbon fiber, which is a violation of the 1-D heat flow assumption of the Parker adiabatic solution given by Eq. (1).

**Table 2. Fiber Thermal Conductivity Values Predicted from the FE Analysis**

| Specified Fiber Conductivity (W/m*K) | Fiber Volume Content (%) | Predicted Fiber Thermal Conductivity (W/m*K) | |
|---|---|---|---|
| | | L = 1 mm | L = 2 mm |
| **10** | **10** | 9.99 | 10.0 |
| | **20** | 9.98 | 10.0 |
| | **60** | 9.97 | 9.99 |
| **100** | **10** | 102 | 100 |
| | **20** | 100 | 100 |
| | **60** | 99.6 | 99.9 |
| **1000** | **10** | 2050 | 1080 |
| | **20** | 1290 | 1040 |
| | **60** | 988 | 996 |

Table 2 also summarizes the fiber thermal conductivity values predicted from the FE analysis for 2 mm thick samples. With the exception of the composites containing the highest conductivity fiber (1000 W/m*K) at 10 and 20% fiber content, the LFA method is able to accurately predict fiber thermal conductivity. However, a comparison of samples with 1 mm and 2 mm thickness shows that an increase in length reduces the over-prediction error that results from preferential conduction in composites made with high conductivity fibers having low fiber content.

The results discussed above were for fiber conductivity values of 10 to 1000 W/m*K that were assumed to be isotropic. However, many fibers, including carbon fibers, display anisotropy. Therefore, the effect of anisotropy in fiber thermal conductivity values was examined by

assigning a value of 10 W/m*K for the fiber radial thermal conductivity, while holding the axial conductivity at 1000 W/m*K. The simulated LFA curves for the anisotropic and isotropic fiber are nearly identical. The difference between predicted half-time for the isotropic and anisotropic composites was only 3% for the 10% fiber content composites and less than 0.1% for fiber content of 20% and higher. These small differences may be explained by the fact that the radial heat flow within the sample is limited primarily not by the fiber thermal properties but by the matrix, which has a radial thermal conductivity ($k_m \sim 0.1$ W/m*K) that is about three orders of magnitude lower than the least conductive fiber ($k_f \sim 10$ W/m*K).

## 5.0 CONCLUSIONS

The following conclusions are drawn from the present study that addressed both experimental and modeling aspects of nanomodified pitch-based carbon fibers:

1. The use of melt mixing was confirmed to be an acceptable method for dispersing carbon nanomodifiers such as SAR MWCNT and carbon black into a mesophase pitch matrix. The addition of these nanomodifiers disrupts the typical radial structure of mesophase pitch carbon fibers reducing the number of split fibers. SAR MWCNTs appear to be more efficient at inhibiting the formation of this type of flaw.
2. A method for capturing high-speed images of a carbon fiber during the single-filament tensile recoil test was established. The addition of nanomodifiers in pitch-based carbon fibers produces compressive/tensile ratios that are statistically greater than those of the pure pitch based fibers.
3. Finite element analysis was used to simulate laser flash analysis on unidirectional carbon fiber-epoxy composites. The heterogeneity of the unidirectional composites, in combination with the unsteady-state nature of the LFA method, was found to potential cause preferential heat flow through the carbon fiber, resulting in an over-prediction of fiber thermal conductivity. This effect is most significant for thinner samples containing higher conductive fibers (~100 to 1000 W/m*K) at lower volume fractions.

## 6.0 REFERENCES


[1] E. Fitzer and L. M. Manocha, "Carbon Reinforcements and Carbon/Carbon Composites", Springer-Verlag Publishers, 1998

[2] J. D. Buckley and D. D. Edie, "Carbon-Carbon Materials and Composites," NASA Reference Publication 1254, 1992

[3] D. Schmidt, K. E. Davidson, L. S. Thiebert, "Evolution of Carbon-Carbon Composites," SAMPE Journal, 32 (4), 44-50, 1996

[4] "Mesophase Pitch-Based Carbon Fibers with Carbon Nanotube Reinforcements" A. A. Ogale*, D. D. Edie, and A. Rao, US Patent 7,153,452, issued Dec 2006

[5] T. Cho, Y. S. Lee, R. Rao, A.M. Rao, D. D. Edie, and A. A. Ogale*, "Structure of carbon fiber obtained from nanotube-reinforced mesophase pitch," Carbon, 41(7), 1419-24, 2003

[6] Young Rack Ahn, Young Seak Lee, A. A Ogale, Chang Hun Yun, Chong Rae Park, "Compressional Behavior of Carbon Nanotube Reinforced Mesophase Pitch-based Carbon Fibers," Fibers and Polymers, 7(10), 85-87, 2006

[7] J. Cribb, Honors Thesis, Department of Chemical and Biomolecular Engineering, Clemson University, May 2011.

[8] W.J. Parker, R.J. Jenkins, C.P Butler, G.L. Abbott, "Flash Method of Determining Thermal Diffusivity, Heat Capacity, and Thermal Conductivity," Appl Phys, **32(9),** 1679-84, 1961

[9] A. A. Ogale, "Novel Pitch Materials for High Thermal Conductivity Carbon Fibers, Foams and Composites: Phase II", Final Report submitted to UTC/AFRL, April 2010

[10] J.G. Lavin, D.R. Boyington, J. Lahijani, B. Nysten, J-P. Issi. "The Correlation of Thermal Conductivity with Electrical Resistivity in Mesophase Pitch-Based Carbon Fiber," Carbon, 31(6),1001-2, 1993

[11] M.K. Alam, A.M. Druma, C. Druma, Thermal Transport in Graphitic Carbon Foams, J. Compos. Mater. 38 (2004) 1993-2006

# LIST OF SYMBOLS, ABBREVIATIONS, AND ACRONYMS

| Acronym | Description |
|---|---|
| AFRL | Air Force Research Laboratory |
| CB | Carbon Black |
| DOD | Department of Defense |
| DTIC | Defense Technical Information Center |
| FEM | Finite Element Modeling |
| FWHM | Full-Width at Half-Maximum |
| LFA | Laser Flash Analysis |
| MIT | Measurement Technology, Inc. |
| MWCNT | Multi-Walled Carbon Nanotubes |
| RVE | Representative Volume Element |
| RX | Materials Directorate |
| RXB | Nonmetallic Materials Division |
| RXBT | Nanostructural Materials Branch |
| SAR | Short Aspect Ratio |
| TOPS | Technical Operations Support |
| USAF | United States Air Force |
| UTC | Universal Technology Corporation |
| WPAFB | Wright-Patterson Air Force Base |